Bulletin of the Seismological Society of America

# Temporal Variation of the Spectral Decay Parameter Kappa Detected Before and After the 2016 Main Earthquakes of Central Italy

--Manuscript Draft--

| | |
|---|---|
| **Manuscript Number:** | BSSA-D-22-00107R2 |
| **Article Type:** | Article |
| **Section/Category:** | Regular Issue |
| **Full Title:** | Temporal Variation of the Spectral Decay Parameter Kappa<br>Detected Before and After the 2016 Main Earthquakes of Central Italy |
| **Corresponding Author:** | Raul Ramon Castro, Ph.D.<br>CICESE<br>Ensenada, Baja California MEXICO |
| **Corresponding Author's Institution:** | CICESE |
| **Corresponding Author E-Mail:** | raul@cicese.mx |
| **Order of Authors:** | Raul Ramon Castro, Ph.D. |
| | Daniele Spallarossa, Ph.D. |
| | Francesca Pacor, Ph.D. |
| | Leonardo Colavitti, Ph.D. |
| | Giovanni Lanzano, Ph.D. |
| | Claudia Andrea Vidales-Basurto, Ph.D. |
| | Sara Sgobba, Ph.D. |
| **Abstract:** | We investigated the temporal variation of the spectral decay parameter κ before and after two main earthquakes that occurred in the central Italy region, namely the Amatrice (Mw 6.0) of August 24, 2016, and the Norcia (Mw 6.5) of October 30, 2016, earthquakes. For this analysis we used seismograms from the Central Italy dense seismic array stations, and earthquakes located at hypocenter distances r < 80 km, having magnitudes Mw 3.4-6.5. The data set consists of 393 events recorded at 92 stations. We estimated for both earthquake sequences average functions that describe the distance dependence of κ along the S-wave source-station paths using acceleration spectra from foreshocks, main shock, and aftershocks. We observed that there was a regional attenuation drop within approximately two months after the Amatrice earthquake. Then, tends to return towards the attenuation values observed before the occurrence of the main event, namely to the values of obtained from the foreshocks, when the earthquake cycle is probably completed. We also estimated the near-source kappa (Ks ) using aftershocks from August 24, 2016, to September 3, 2016. The results show that near the epicenter of the Amatrice earthquake the values of are lower than those from aftershocks located to the north, suggesting that the tectonic stress was probably high near the rupture zone and that there may be a likely fluid-flow of crustal fluids. obtained from the foreshocks of the Norcia earthquake is like that calculated with the records of the Amatrice aftershocks. Then, drops to lower attenuation values during the Norcia main event and tends to increase again during the aftershocks. From the analysis of these two earthquake sequences, that occurred in a short time interval in central Italy, we conclude that the temporal variation of could be a valuable indicator to monitor the earthquake cycle. |
| **Author Comments:** | No comments |
| **Suggested Reviewers:** | Edoardo Del Pezzo, Ph.D.<br>Professor, Istituto Nazionale di Geofisiaca e Vulcanologia, Osservatorio Vesuviano, Napoli, Italy<br>edoardo.delpezzo@ingv.it<br>He is an expert in seismic attenuation and has published papers related with that topic in the same region of our paper (central Italy). |
| | |

| | |
|---|---|
| | Simona Gabrielli, Ph.D.<br>Senior Research Seismologist, Istituto Nazionale di Geofisiaca e Vulcanologia, Roma, Italy<br>simona.gabrielli@ingv.it<br>She has been studied the 2016 earthquake sequence of central Italy and has a paper that relates with our major results. She may be interested in reviewing our paper. |
| **Opposed Reviewers:** | |
| **Response to Reviewers:** | We made the following changes in response to Editor's comments and suggestions:<br><br>•We changed the title to make it a complete sentence and to provide more information about the content of the paper.<br>•All the magnitudes that we refer to in the text are moment magnitude. We replace M to Mw throughout the paper.<br>•We rephrased the text on line 23 and made the changes that you requested on lines 90, 101 and 460 (and the caption of Figure 3).<br>•We removed the color bar of figure 1 and used circles of different diameter and color according to the magnitudes. We also made both maps equal size and show the inset in only one of them (top map). The inset was also modified to show only Europe.<br>•We changed the color-bar of figure 5 to emphasize the different values of kappa (Ks).<br>•We added in the caption of Figure 6 that the line corresponds to the best-fitting regression, and we added in lines 225-227, of the revised manuscript, that the line in Figure 6 is the best-fitting linear regression, which has a negative correlation coefficient of -0.38, indicating a weak correlation between   and focal depth (H). |
| **Additional Information:** | |
| **Question** | **Response** |
| <b>Key Point #1: </b><br><i>Three key points will be printed at the front of your manuscript so readers can get a quick overview. Please provide three COMPLETE sentences addressing the following: 1) state the problem you are addressing in a FULL sentence; 2) state your main conclusion(s) in a FULL sentence; and 3) state the broader implications of your findings in a FULL sentence. Each point must be 110 characters or less (including spaces). | Temporal variation of the decay parameter κ before and after the 2016 earthquakes in central Italy |
| **Key Point #2:** | The variation of the average $\tilde{\kappa}$(r) along the path can be related to fluid flow in the seismogenic zone |
| **Key Point #3:** | The temporal variation of $\tilde{\kappa}$(r) may be a good indicator to monitor the earthquake cycle |

Dr. Raúl R. Castro
CICESE, Dep. Sismología
Ensenada, Baja California
22860, México
Email: raul@cicese.mx

Prof. P. Martin Mai
Editor-in-Chief
Bulletin of the Seismological Society of America

September 22, 2022

Dear Prof. Mai,

We are submitting the revised manuscript titled "*Temporal Variation of the Spectral Decay Parameter Kappa Detected Before and After the 2016 Main Earthquakes of Central Italy"*, by Castro, Spallarossa, Pacor, Colavitti, Lanzano, Vidales-Basurto and Sgobba accepted for publication in the *Bulletin of the Seismological Society of America.* We are also including two cover photos so that you can choose the best for the cover image, in addition to the final figures.

We made the following changes in response to your comments and suggestions:

- We changed the title to make it a complete sentence and to provide more information about the content of the paper.
- All the magnitudes that we refer to in the text are moment magnitude. We replace M to Mw throughout the paper.
- We rephrased the text on line 23 and made the changes that you requested on lines 90, 101 and 460 (and the caption of Figure 3).
- We removed the color bar of figure 1 and used circles of different diameter and color according to the magnitudes. We also made both maps equal size and show the inset in only one of them (top map). The inset was also modified to show only Europe.
- We changed the color-bar of figure 5 to emphasize the different values of kappa (*Ks*).
- We added in the caption of Figure 6 that the line corresponds to the best-fitting regression, and we added in lines 225-227, of the revised manuscript, that the line in Figure 6 is the best-fitting linear regression, which has a negative correlation coefficient of -0.38, indicating a weak correlation between $\kappa_s$ and focal depth (H).

We are looking forward to seeing our paper published in the *BSSA.*

Sincerely,

Raúl R. Castro

Cover Image (photograph to be considered for the cover of BSSA) | Click here to access/download;Cover Image (photograph to be considered for the cover of BSSA);02_Amatrice.jpg

Cover Image (photograph to be considered for the cover of BSSA)

Click here to access/download;Cover Image (photograph to be considered for the cover of BSSA);03_Norcia.jpg

September 22, 2022

Dear Prof. Mai,

We made the following changes in response to your comments and suggestions:

- We changed the title to make it a complete sentence and to provide more information about the content of the paper.
- All the magnitudes that we refer to in the text are moment magnitude. We replace M to Mw throughout the paper.
- We rephrased the text on line 23 and made the changes that you requested on lines 90, 101 and 460 (and the caption of Figure 3).
- We removed the color bar of figure 1 and used circles of different diameter and color according to the magnitudes. We also made both maps equal size and show the inset in only one of them (top map). The inset was also modified to show only Europe.
- We changed the color-bar of figure 5 to emphasize the different values of kappa (*Ks*).
- We added in the caption of Figure 6 that the line corresponds to the best-fitting regression, and we added in lines 225-227, of the revised manuscript, that the line in Figure 6 is the best-fitting linear regression, which has a negative correlation coefficient of -0.38, indicating a weak correlation between $\kappa_s$ and focal depth (H).

Raúl R. Castro

# *Temporal Variation of the Spectral Decay Parameter Kappa Detected Before and After the 2016 Main Earthquakes of Central Italy*

Raúl R. Castro[1], Daniele Spallarossa,

Francesca Pacor , Leonardo Colavitti, Giovanni Lanzano,

Claudia A. Vidales-Basurto and Sara Sgobba

[1]*Centro de Investigación Científica y de Educación Superior de Ensenada (CICESE), División Ciencias de la Tierra, Departamento de Sismología, Carretera Tijuana-Ensenada No. 3918, 22860 Ensenada, Baja California, México.* raul@cicese.mx

**Declaration of Competing Interests**

The authors acknowledge there are no conflict of interest recorded.

**Abstract**

We investigated the temporal variation of the spectral decay parameter $\kappa$ before and after two main earthquakes that occurred in the central Italy region, namely the Amatrice (Mw 6.0) of August 24, 2016, and the Norcia (Mw 6.5) of October 30, 2016, earthquakes. For this analysis we used seismograms from the Central Italy dense seismic array stations, and earthquakes located at hypocenter distances $r$ < 80 km, having magnitudes Mw 3.4-6.5. The data set consists of 393 events recorded at 92 stations. We estimated for both earthquake sequences average functions $\tilde{\kappa}(r)$ that describe the distance dependence of $\kappa$ along the *S*-wave source-station paths using acceleration spectra from foreshocks, main shock, and aftershocks. We observed that there was a regional attenuation drop within approximately two months after the Amatrice earthquake. Then, $\tilde{\kappa}(r)$ tends to return towards the attenuation values observed before the occurrence of the main event, namely to the values of $\tilde{\kappa}(r)$ obtained from the foreshocks, when the earthquake cycle is probably completed. We also estimated the near-source kappa ($\kappa_S$) using aftershocks from August 24, 2016, to September 3, 2016. The results show that near the epicenter of the Amatrice earthquake the values of $\kappa_S$ are lower than those from aftershocks located to the north, suggesting that the tectonic stress was probably high near the rupture zone and that there may be a likely fluid-flow of crustal fluids. $\tilde{\kappa}(r)$ obtained from the foreshocks of the Norcia earthquake is like that calculated with the records of the Amatrice aftershocks. Then, $\tilde{\kappa}(r)$ drops to lower attenuation values during the Norcia main event and tends to increase again during the aftershocks. From the analysis of these two earthquake sequences, that occurred in a short time interval in central Italy, we conclude that the temporal variation of $\tilde{\kappa}(r)$ could be a valuable indicator to monitor the earthquake cycle.

**Key points:**

1. Temporal variation of the decay parameter $\kappa$ before and after the 2016 earthquakes in central Italy
2. The variation of the average $\tilde{\kappa}(r)$ along the path can be related to fluid flow in the seismogenic zone
3. The temporal variation of $\tilde{\kappa}(r)$ may be a good indicator to monitor the earthquake cycle

## Introduction

Several geophysical investigations have shown that the temporal and spatial distribution of aftershocks seem to correlate with physical mechanisms that are time-dependent, such as state friction (Dieterich, 1972), after slip (Burgmann *et al*., 2002), poroelastic rebound (Jónsson *et al*., 2003) and static stress drop estimates (Kemma *et al*., 2021). Recent studies have suggested that changes in pore pressure can induce crustal stresses a few months after a strong earthquake (Albano *et al*., 2019; Convertito *et al*., 2020). These changes in pore pressure can explain the spatial and temporal distributions of aftershocks (Nur and Booker, 1972; Bosl and Nur, 2002; Albano *et al*., 2017; among others). Moreover, to explain the decay of the number of aftershocks with time, usually observed during earthquake sequences, Nur and Booker (1972) proposed that the presence of a viscous element is necessary, and they show that the flow of pore fluid provides this viscous component. Because the presence of fluids in the crust can increase *S*-wave attenuation, a spatial and temporal variability of the spectral decay parameter kappa ($\kappa$) is expected. *Q*-tomography studies in the central Italy region (Chiarabba *et al*., 2009; Amoroso *et al*., 2017) show attenuation and velocity heterogeneities that may be related to fluid-pressure migration in the fault system of this region. Previous studies of seismic attenuation (Castro *et al*., 2000) in the Umbria-Marche region of central Italy show significant variability of the parameter $\kappa$ that could be related also to the presence of fluids in the crust.

In this paper, we study the temporal variation of the spectral decay parameter $\kappa$ in central Italy using earthquakes from the Amatrice-Norcia 2016 seismic sequence. The Amatrice (Mw 6.0) earthquake ($42^0$ 42'N, $13^0$ 13.8'E) occurred on 24 August 2016 and caused severe damage and casualties in the village of Amatrice (Chiaraluce *et al*., 2017; Fiorentino *et al*., 2018). Many aftershocks were reported to occur for several days which gradually migrated to the north from the epicentral area of the initial rupture, suggesting that a diffusive transit process was taking place, perhaps related to the flow of pore fluids (Tung and Masterlark, 2018; Albano *et al*., 2019). After the Amatrice main shock, it is likely that the flow of fluids reduced the stability of the fault system and triggered the sequence (Gabrielli *et al*., 2022), including the Mw 5.9 earthquake of October 26, 2016, that occurred near the village of Visso ($42^0$ 54.6'N, $13^0$ 7.8'E), and on 30 October a larger event (Mw 6.5) that occurred on the town of Norcia ($42^0$ 49.8'N, $13^0$ 6.6'E) causing further damage. The red stars in Figure 1a are the epicentral locations of these earthquakes.

There are several factors that may impact the estimates of the attenuation parameter $\kappa$, particularly to the near-surface component $\kappa_0$. Ktenidou *et al*. (2013) investigated the variability of $\kappa$ in a vertical array that recorded earthquakes at a downhole and found a significant variability of $\kappa_0$ at the surface and at the rock sites. Perron *et al*. (2017) used a semiautomatic procedure to measure $\kappa$ and show that the associate uncertainty of the estimates of $\kappa$ depend on the bandwidth use to determine $\kappa$. They also found that site amplification has an important impact in the estimate of $\kappa_0$. Hollender *et al*. (2020) found that soil-structure interaction may cause high-frequency amplifications that can affect the estimation of $\kappa$. However, this effect can be considered part of the $\kappa_0$ component of $\kappa$. Parolai and Bindi (2004) show that site effects may not affect the determination of $\kappa$ when the site resonances are below the frequency band used to calculate $\kappa$.

We focus on this paper in the average regional source-station path contribution of $\kappa$ ($\tilde{\kappa}(r)$) and minimize the uncertainties of the $\kappa$ estimates by making a careful selection of the data used. Most of the records analyzed come from sites having frequency resonances outside of the frequency band used to calculate $\kappa$ ($f$ = 8-38 Hz) and the selected earthquakes (Mw>3.4) have corner frequencies considerably lower than 8 Hz. In addition, we used an inversion technique that separates source, path and site effects from the estimates of $\kappa$ (e.g. Van Houtte *et al*., 2011)

## Data

We analyzed accelerograms and velocity records from the Central Italy dense seismic array stations that recorded the 2016 Amatrice (Mw 6.0), and the Norcia (Mw 6.5) earthquake sequences. The data set consists of 393 earthquakes located at hypocenter distances $r < 80$ km, having magnitudes 3.4< Mw< 6.5, recorded by 92 stations (Figure 1b) from the Italian National Seismic Network (RSNC), that is managed by the *Istituto Nazionale di Geofisica e Vulcanologia* (INGV), and the National Accelerometric Network (RAN), that is managed by the Civil Protection Department (DPC). Most stations are on class B sites ($V_{S\_30}$=360-800 m/s), using EC8 site classification, and the natural frequency of resonance is between 3 Hz and 6.7 Hz, outside the frequency band (8-38 Hz) used to calculate $\kappa$. The magnitude-distance distribution of the recordings is displayed in Figure 2. Most of the events have a magnitude Mw < 4.9 and have epicentral distances of less than 140 km.

We selected earthquakes having records with signal-to-noise ratio (SNR) greater than three and that were recorded for more than 50 stations to assure that the earthquake locations are reliable. Moreover, the earthquakes selected (Mw > 3.4) have corner frequencies lower than the frequency band (8 – 38 Hz) used to estimate $\kappa$. It is expected that for earthquakes with Mw > 3.4 the corner frequency ($f_c$) is considerably lower than 8 Hz (Aki, 1987). For instance, the rupture length of an Mw=3.5 event is approximately 0.26 km (Wells and Coppersmith, 1994), and that gives an $f_c$ =4.35 Hz, using Brure (1970) source model, larger earthquakes have smaller $f_c$.

The time series are generally sampled at 100 samples per second and are baseline corrected by subtracting the average of all points following the same method as Pacor *et al*. (2016). The *S*-

wave spectral amplitudes were calculated with time windows selected using a distance-dependent energy criterion. A 4 s minimum length was used for close hypocenter-distance range, to be able to resolve above 1 Hz. The windows start 0.1 s before the direct *S*-wave arrival and end when the accumulated energy reaches 90% of the total recording for $r < 25$ km, 80% for 25-50 km and 70% for $r > 50$ km. These windows contain primarily *S* waves and avoid surface-wave contamination. Finally, the selected windows are tapered with a Hanning window, and the spectral amplitudes are smoothed using $b=40$ with the Konno and Ohmachi (1998) technique. We combine the north-south (N-S) and the east-west components ($A(f) = \sqrt{A(f)_{N-S}^2 + A(f)_{E-W}^2}$ ) to estimate $\kappa$.

**Method**

We computed $\kappa$ using a similar method introduced by Anderson and Hough (1984), where the logarithm of the high-frequency *S*-wave spectral amplitude acceleration is least-squares fitted and $\kappa$ is estimated from the slope of the linear fit which equals $-\pi Log(e)\kappa$. We estimated the median $\kappa$ and the corresponding standard deviation with a semi-automatic technique that precompute the slopes over 11 frequency bands with length varying between 8 and 38 Hz (Lanzano *et al*., 2022). The parameter $\kappa$ is calculated via the least-square fit if at least 65% of the spectral ordinates exceed a signal-to-noise ratio (SNR) threshold of three, and if the lowest frequency of the band is larger than the corner frequency of the theoretical Brune's spectrum of the event, computed considering a typical stress drop value of 3 MPa for central Italy (Bindi *et al*., 2004) and $V_S$=3.0 km/s, the average crustal velocity value based on the standard model of central Italy (De Luca *et al*., 2009). The median value of $\kappa$ is discarded if it was pre-computed with less than six of the 11 frequency bands considered and if the associated standard deviation is larger than 0.015 s (the observed variability of $\kappa$ at a given distance). The variability of $\kappa$ is estimated by selecting $\kappa$ from records having the same hypocenter distance and calculating the standard deviation.

The resulting values of $\kappa$ were modeled following Anderson (1991), Ktenidou *et al.* (2014) and Castro *et al.* (2022) as:

$$\kappa(\kappa_s, r, \kappa_0) = \kappa_s + \tilde{\kappa}(r) + \kappa_0 \qquad (1)$$

Where $\kappa_s$ is the attenuation near the source, $\tilde{\kappa}(r)$ is the average attenuation along the *S*-wave source-station distance $r$ and $\kappa_0$ is the attenuation near the site. A similar inversion scheme was previously introduced by Van Houtte *et al.* (2011) to separate source, site and path contributions to $\kappa$.

We determined first $\tilde{\kappa}(r)$ with the nonparametric technique proposed by Anderson (1991), which defines a function that describes the variation of $\kappa$ with distance without assuming an *a priori* functional form. For that purpose, eq. (1) can be rewritten as (Castro *et al.*, 2022):

$$\kappa(r) = \kappa_1 + \tilde{\kappa}(r) \qquad (2)$$

Where $\kappa_1$ includes both the attenuation near the source and near the site. To solve eq. (2) it is assumed that $\tilde{\kappa}(r)$ is a smooth function of $r$, that $\kappa$ varies slowly with distance, that $\tilde{\kappa}(0) = 0,$ and that the shape remains the same for all the earthquakes and that undulations in the observed $\kappa$ are related to $\kappa_1$. The function $\tilde{\kappa}(r)$ is shifted downward or upward, depending on the value of $\kappa_1$. This empirical model provides curves that are unbiased by *a priori* assumptions about the nature of the distance dependence of $\tilde{\kappa}(r)$ (e.g., Anderson, 1991).

We estimate $\kappa_1$ in a second iteration by correcting the observed values of $\kappa$ with the function $\tilde{\kappa}(r)$ obtained solving eq. (2). Then, we solved the following system of equations as in Castro *et al.* (2022):

$$\kappa_{1ij} = \kappa_{0i} + \kappa_{sj} \quad (3)$$

Where $\kappa_{1ij}$ is the corrected value, by the average path attenuation ($\tilde{\kappa}(r)$), of the observed $\kappa$ from site *i* and source *j*; $\kappa_{0i}$ is the near-site attenuation parameter at station *I*; and $\kappa_{sj}$ is the near-source attenuation from earthquake *j*. To resolve the degree of freedom between $\kappa_{0i}$ and $\kappa_{sj}$, we constrained eq. (3) to satisfy the condition:

$$\sum_{i=1}^{N} \kappa_{0i} = 0 \quad (4)$$

where *N* is the number of reference sites used for that constraint. Note that this constraint is irrelevant for the analysis of $\tilde{\kappa}(r)$, which is our primary interest. The values of $\kappa_{0i}$ of the reference sites vary between 0.0049 and 0.0183.

## Results and Discussion

### *The Amatrice (Mw 6.0) of 24 August 2016 and the Visso (Mw 5.9) of 26 October Earthquakes*

Figure 3 (left) shows the average attenuation along the *S*-wave path $\tilde{\kappa}(r)$ obtained using estimates of $\kappa$ from stations that recorded the Amatrice main event (solid line). These values of $\kappa$ are like those obtained by Castro *et al*. (2000) using earthquakes from the Umbria-Marche, central Italy region, namely, 0.026 to 0.057 s between 20 and 83 km. These values of $\kappa$ are also consistent with the mean value of 0.005 s obtained by Bindi *et al*. (2004) in the same region. We also computed $\tilde{\kappa}(r)$ using records from one foreshock recorded on January 18, 2016, about seven months before the main event (asterisks), and from aftershocks that occurred for 15 days (circles), 30 days (triangles), 2 months (diamonds) and 3 months (crosses) after the main earthquake. The estimates of $\tilde{\kappa}(r)$ using aftershocks from 15-30 days and 3 months, as well as those from the Norcia aftershocks are within the error bars of the corresponding estimates. For the Visso sequence, the error bars overlap between foreshocks and aftershocks (Figure 3).

Based on these results, it seems that the attenuation in the epicentral area remain approximately unchanged (3 % increased) for at least seven months before the main earthquake. During the Amatrice sequence Gabrielli *et al*. (2022) observed high scattering, which is consistent with the high values of $\tilde{\kappa}(r)$ showing in Figure 3 (left) before and during the main shock. An increase in attenuation is expected during main earthquakes due to rock damage, generated by the fault rupture, that increases rock permeability (Ben-Zion and Ampuero, 2009; Kelly *et al*., 2013; Castro and Ben_Zion, 2013; Malagnini and Parsons, 2020) allowing fluid flow. When rocks are water saturated the friction coefficient decreases facilitating sliding and thus decreasing the quality factor $Q$ of the $S$ waves significantly and increasing at the same time the overall attenuation (Johnston *et al*., 1979). Then, $\tilde{\kappa}(r)$ gradually decreased by 39 % after the first 30 days of the main earthquake and then the attenuation dropped considerably (85 %) after two months. It is possible that after the main event fluids flowed outside of the epicentral area and the stress drop produced by the main shock reduced the permeability of the rocks with a consequent reduction of attenuation. Malagnini *et al*. (2022) observed a notable decrease of $Q_S^{-1}(f,t)$ after normal faulting earthquakes of central Italy. After this period, $\tilde{\kappa}(r)$ start increasing for the next month, probably due to fluids redistribution. Two months after the Amatrice main event the aftershocks migrated 20 km north (Chiaraluce *et al*., 2017; Tung and Masterlak, 2018) and triggered the Visso (M5.9) mainshock. Figure 3 (right) shows that $\tilde{\kappa}(r)$ had approximately the same attenuation level before the Visso main event as the three-month aftershocks of the Amatrice earthquake, and $\tilde{\kappa}(r)$ also decreased during the Visso aftershocks as shown on the right of Figure 3 (circles).

A possible explanation of the temporal variation of $\tilde{\kappa}(r)$ can be related to stress variations and changes in the elastic properties of the medium, as part of a post-event phase. These changes of $\tilde{\kappa}(r)$ could be also related to the migration of pressurized fluids in the epicentral area (e.g., Lucente *et al*., 2010). Several authors (Miller *et al*., 2004; Chiodini *et al*., 2004; Di Luccio *et al*., 2010; Malagnini *et al*., 2012) have proposed that $CO_2$-rich fluids and gas releases modulate the seismicity in the Central Italy region. Changes in permeability of the rocks during seismic sequences can produce attenuation variations and create fluid-flow pathways that can contribute to the triggering of mainshock sequences (Malagnini *et al*., 2022).

We also computed the near-source kappa ($\kappa_s$) using aftershocks from August 24, 2016, to September 3, 2016, and the two-step inversion described above. These events are well azimuthally recorded to assure that the estimates of $\kappa_s$ are not affected by possible anisotropy of $\tilde{\kappa}(r)$. Figure 4 shows the values of $\kappa_s$ plotted chronologically. The errors of the $\kappa_s$ estimates range between 0.0005 and 0.0024, less than 13% of the estimated values of $\kappa_s$.

The spatial variability of $\kappa_s$ after the Amatrice earthquake, is shown in Figure 5, where the blue star represents the epicenter of the main event and the circles the location of the aftershocks. Near the epicenter of the main event the values of $\kappa_s$ are lower than those from aftershocks located north from the main event. This suggests that the tectonic stress was probably high near the rupture zone. Experimental data shows that attenuation decreases with increasing pressure (Johnston *et al*., 1979). Figure 6 (left) shows that $\kappa_s$ tends to increase when the focal depth of the aftershocks decreases, probably because crustal permeability decreases with depth, favoring the presence of fluid-saturated rocks in the upper crust (Tung and Masterlark, 2018). The errors of the focal depth (H) vary between 0.2 and 0.7 km, less than 10% of H. The line is the best-fitting linear regression, which has a negative correlation coefficient of -0.38, indicating a weak correlation between $\kappa_s$ and

H. Figure 6 (right) displays the distribution of $\kappa_s$ with earthquake magnitude and shows that earthquakes in the magnitude range of 3.5 to 4.0 have wide variability of attenuation near the source. However, for larger magnitude (Mw>4) events $\kappa_s$ seems to increase from 0.0046 for Mw=4.0 to 0.0147 for Mw=6.3, although the apparent increasing trend is not clear. It is possible that larger magnitude events may generate a bigger rock-damage area increasing the rock permeability and facilitating the presence of fluids.

*The Norcia Earthquake (Mw 6.5) of 30 October 2016*

For this earthquake sequence, we analyzed foreshocks that occurred from October 8, 2016, to October 29, 2016, one day before the main event, and aftershocks that occurred from October 30, at 06:40 hrs., eight minutes after the main event, to November 16, 2016.

Figure 7 shows the resulting $\tilde{\kappa}(r)$ functions obtained from the foreshocks (continuous line), the main event (triangles) and the aftershocks (stars). The error bars of the estimates of $\tilde{\kappa}(r)$ vary between 0.00096 and 0.00397 s. The values of $\tilde{\kappa}(r)$ from the foreshocks is within the values of the $\tilde{\kappa}(r)$ functions obtained from the Amatrice aftershocks (filled squares in Figure 3 left), suggesting that the state of stress and the elastic properties of the media tend to return to the prevailing conditions after the Amatrice earthquake. The Norcia main event generated a significant attenuation drop, possibly related with an increase in tectonic stress and migration of fluids outside of the epicentral zone. Gabrielli *et al*. (2022) observed low scattering during the Norcia sequence which traduces into low attenuation and low $\tilde{\kappa}(r)$. The values of $\tilde{\kappa}(r)$ from the aftershocks show that the attenuation increased probably during the recuperation phase of the elastic properties of the media after the main event and after completing the earthquake cycle.

## Conclusions

From the analysis of two earthquake sequences, that occurred in a short time interval in central Italy, we estimated average functions $\tilde{\kappa}(r)$ that describe the distance dependence of the spectral decay parameter $\kappa$ along the *S*-wave source-station paths. We observed a regional drop of the attenuation parameter $\kappa$ within approximately two months after the Amatrice earthquake (Mw 6.0) of 24 August 2016. Then, $\tilde{\kappa}(r)$ tends to return towards the attenuation values observed before the occurrence of the main event, namely to the values of $\tilde{\kappa}(r)$ obtained from the foreshocks, when the earthquake cycle is likely completed. Because $\tilde{\kappa}(r)$ obtained from the foreshocks of the Norcia earthquake (Mw 6.5) of 30 October 2016 is comparable to that calculated with records from the Amatrice aftershocks, it is likely that at that point the tectonic stress returned to its original state. Then, $\tilde{\kappa}(r)$ drops during the Norcia main event and tends to increase again during the aftershock sequence. A possible explanation of this temporal variability of the regional $\tilde{\kappa}(r)$ is that during the Amatrice earthquake sequence the rock damage generated by the foreshocks increased the rock permeability permitting the crustal fluids to flow, decreasing the friction coefficient, and facilitating sliding (Figure 3 left). After the main event the fluids migrated towards the Visso epicentral area saturating the rocks, making the quality factor *Q* of *S* waves significantly lower and increasing the attenuation (Figure 3 right). In the meantime, the tectonic stress was transferred to the Norcia region generating the foreshocks and eventually the main event. The Norcia mainshock increased the fracturing and allowed crustal fluids to flow facilitating the triggering of the aftershocks and increasing the attenuation (Figure 7).

The near source $\kappa_s$ is low near the epicenter of the Amatrice earthquake, increasing towards the north and south of the epicenter (Figure 5). This, together with the observed temporal variations of $\tilde{\kappa}(r)$ indicates that fluid flow must be an important factor controlling the rupture process. For instance, Gabrielli *et al*. (2022) observed that the evolution of seismic sequences across the Apennines are consistent with the role of fluids with high $CO_2$ content, as reported by other authors (Miller *et al*., 2004; Chiodini *et al*., 2004; Di Luccio *et al*., 2010; Malagnini *et al*., 2012).

We conclude that the temporal variation of $\tilde{\kappa}(r)$ could be a good indicator to monitor the earthquake cycle in central Italy.

## Acknowledgements

This research was supported by INGV in the frame of the project "*Pianeta Dinamico*". Working Earth project – Geosciences for the Understanding of the Dynamics of the Earth and the Consequent Natural Risks (CUP code D53J19000170001), funded by MIUR (Italian Ministry of University and Research) aimed at the relaunch of investments of the central administrations of the State and development of the country) – Task S3 – 2021. – regarding the Seismic attenuation and variability of seismic motion. I thank the technical support provided by Antonio Mendoza Camberos and Arturo Pérez Vertti from the Earth Science Division, Department of Seismology of CICESE. A special acknowledgment to the Associate Editor Dr. Adrian Oth, the Editor-in-Chief Prof. P. Martin Mai and the two anonymous reviewers for their comments and suggestions that help us to improve the manuscript.

## Data and Resources

The data used comes from permanent networks operated by the INGV (Istituto Nazionale di Geofisica e Vulcanologia): the National Seismic Network (RSN) and the Mediterrean Network (Mednet); the Rapid Response Networks that are operated together with the University of Genova and the RESIF (*Réseau Seismologique et Géodésique Français*). Other permanent stations belong to the National Accelerometric Network (RAN), operated by the Department of Civil Protection. The acceleration records can be obtained from the Italian Accelerometric Archive (http://itaca.mi.ingv.it), and the velocity records from the European Integrated Data Archive (EIDA; http://eida.rm.ingv.it). Some plots were made using Generic Mapping Tools (http://www.soest.hawaii.edu/gmt; Wessel and Smith, 1998), and with GeoMapApp (http://www.geomapapp.org).

## Declaration of Competing Interests

The authors declare no competing interests.

## References

Albano, M., S. Barba, G. Solaro, A. Pepe, C. Bignami, M. Moro, M. Saroli, and S. Stramondo (2017). Aftershocks, groundwater changes and postsesimic ground displacements related to pore pressure gradients: Insights from the 2012 Emilia Romagna earthquake, *J. Geophys. Res. – Solid Earth*, **112**, 5622-5638, doi: 10.1002/2017JB014009.

Albano, M., S. Barba, M. Saroli, M. Polcari, C. Bignami, M. Moro *et al*. (2019). Aftershock rate and pore fluid difusión: Insights from the Amatrice-Visso-Norcia (Italy) 2016 seismic sequence, *Jour. Geophys. Res. Solid Earth*, **124** 995-1015.

Aki, K. (1987). Magnitude-frequency relation for small earthquakes: A clue to the origin of Fmax of large earthquakes, *J. Geophys. Res*., **92**(B2), 1349-1355.

Amoroso, O., G. Russo, G. De Landro, A. Zollo, S. Garambois, S. Mazzoli, M. Parente, and J. Virieux (2017). From velocity and attenuation tomography to rock physical modeling: Inferences on fluid- driven earthquake processes at the Irpinia fault system in southern Italy. *Geophysical Research Letters*, *44*(13), 6752-6760. https://doi.org/10.1002/2016GL072346.

Anderson, J.G., and S.E. Hough (1984). A model for the shape of the Fourier amplitude spectrum of acceleration at high frequencies, *Bull. Seismol. Soc. Am.*,**74** 1969-1984.

Anderson, J. G. (1991). A preliminary descriptive model for the distance dependence of the spectral decay parameter in southern California, *Bull. Seismol. Soc. Am*., **81** 2186-2193.

Ben-Zion, Y., and J. Ampuero (2009). Seismic radiation from regions sustaining material damage, *Geophys. J. Int*. **178**, 1351–1356, doi: 10.1111/j.1365-246X.2009.04285.x.

Bindi, D., R.R. Castro, G. Franceschina, L. Luzi, and F. Pacor (2004). The 1997-98 Umbria-Marche sequence (Central Italy): source, path and site effects estimated from strong motion data recorded in the epicentral area, *Jour. of Geophys. Res.*, **109**, B04312, 1-17.

Bosl, W. J., and Nur, A. (2002). Aftershocks and pore fluid diffusion following the 1992 Landers earthquake, *J. Geophys. Res. – Solid Earth*, 107 (B12), ESE 17-1-ESE 17-12. doi: 10.1029/2001JB000155.

Brune, J.N. (1970) Tectonic stress and the spectra of seismic shear waves from earthquakes. *Jour Geophys Res* **75,** 4997-5009.

Bürgmann, R., S. Ergintav, P. Segall, E.H. Hearn, S. McClusky, R.E. Reilinger, et al. (2002). Time- dependent distributed afterslip on and deep below the Izmit earthquake rupture, *Bull. Seismol. Soc. Am.*, **92** 126–137. https://doi.org/10.1785/ 0120000833.

Castro, R. R., and Y. Ben-Zion (2013). Potential signatures of damage-related radiation from aftershocks of the 4 April 2010 (Mw 7.2) El Mayor-Cucapah earthquake, Baja California, México, *Bull. Seism. Soc. Am.*, **103**, 1130-1140.

Castro, R.R., L. Trojani, G. Monachesi, M. Mucciarelli, and M. Cattaneo (2000). The spectral decay parameter $\kappa$ in the region of Umbria-Marche, Italy, *Jour. Geophys. Res.*, **105** 23,811-23,823.

Castro, R.R., L. Colavitti, C.A. Vidales-Basurto, F. Pacor, S. Sgobba, and G. Lanzano (2021). Near-source attenuation and spatial variability of the spectral decay parameter kappa in Central Italy *Seism. Res. Lett.* (in press).

Chiarabba, C., D. Piccinini, and P. De Gori (2009). Velocity and attenuation tomography of the Umbria Marche 1997 fault system: Evidence of a fluid-governed seismic sequence. *Tectonophysics* **476** 73-84.

Chiaraluce, L., R. Di Stefano, E. Tinti, L. Scognamiglio, M. Michele, E. Casarotti, et al. (2017). The 2016 central Italy seismic sequence: A first look at the mainshocks, aftershocks, and source models. *Seism. Res. Lett*. **88** 757–771. https://doi.org/10.1785/ 0220160221.

Chiodini, G., C. Cardellini, A. Amato, E. Boschi, S. Caliro, F. Frondini, and G. Ventura (2004). Carbon dioxide Earth degassing and seismogenesis in central and southern Italy. *Geophys. Res. Lett*., **31**(7). https://doi.org/10.1029/2004GL019480.

Convertito, V., R. De Matteis, L. Improta, N. A. Pino (2020). Fluid-Triggered Aftershocks in an Anisotropic Hydraulic Conductivity Geological Complex: The Case of the 2016 Amatrice Sequence, Italy. *Frontiers in Earth Science – Solid Earth Geophysics.* https://doi.org/10.3389/feart.2020.541323.

De Luca, G., M. Cattaneo, G. Monachesi, A. Amato (2009). Seismicity in Central and Northern Apennines integrating the Italian national and regional networks. *Tectonophysics*, **476** 121-135.

Dieterich, J. H. (1972) Time- dependent friction in rocks. *Jour. of Geophys. Res*., **77** 3690–3697. https://doi.org/10.1029/ JB077i020p03690.

Di Luccio, F., G. Ventura, R. Di Giovambattista, A. Piscini, and F.R. Cinti (2010). Normal faults and thrusts reactivated by deep fluids: The 6 April 2009 Mw 6.3 L'Aquila earthquake, central Italy. *J. Geophys. Res. Solid Earth*, **115**. https://doi.org/10.1029/2009JB007190.

Fiorentino, G., A. Forte, E. Pagano, F. Sabetta, C. Baggio, D. Lavorato, C. Nuti, and S. Santini (2018). Damage patterns in the town of Amatrice after August 24th 2016 Central Italy earthquakes. *Bull. Earthq. Eng*. **16**(3), 1399-1423, https://doi.org/10.1007/s10518-017-0254-z.

Gabrielli, S., A. Akinci, G. Ventura, F. Napolitano, E. Del Pezzo, and L. De Siena (2022). Fast changes in seismic attenuation due to fracturing and fluid migration during the 2016-2017 Central Italy seismic sequence. *Frontiers in Earth Science – Structural Geology and Tectonics* https://doi.org/10.3389/feart.2022.909698.

Hollender, F., Z., Roumelioti, E., Maufroy, P., Traversa, A. Mariscal, (2020). "Can We Trust High- Frequency Content in Strong- Motion Database Signals? Impact of Housing, Coupling, and Installation Depth of Seismic Sensors". *Seism. Res. Lett*. **91**, 2192-2205. doi:10.1785/0220190163

Johnston, D.H., M.N. Toksoz, and A. Timur (1979). Attenuation of seismic waves in dry and saturated rocks: I. Mechanism. *Geophysics*. **44** 691-711.

Jónsson, S., P. Segall, R. Pedersen, and G. Björnsson (2003). Post- earthquake ground movements correlated to pore- pressure transients. *Nature*, **424**(6945): 179–183. https://doi.org/10.1038/nature01776.

Kelly, C.M., A.D. Rietbrock, R. Faulkner, and R.M. Nadeau (2013). Temporal changes in attenuation associated with the 2004 M6.0 Parkfield earthquake, *J. Geophys. Res. Solid Earth*, **118**, 630–645, doi:10.1002/jgrb.50088.

Kemna, K. B., Verdecchia, A., and Harrington, R. M. (2021). Spatio-Temporal Evolution of Earthquake Static Stress Drop Values in the 2016-2017 Central Italy Seismic Sequence. *J. Geophys. Res.: Solid Earth*, **126**, e2021JB022566, doi:10.10: 29/2021JB022566.

Konno, K., and T. Ohmachi (1998). Ground-motion characteristics estimated from spectral ratio between horizontal and vertical components of microtremor. *Bull. Seism. Soc. Am*., **88**(1), 228-241.

Ktenidou, O.-J., C., Gelis, L.-F., Bonilla (2013). A study on the variability of kappa in a borehole: Implications of the computation process. *Bull. Seimol. Soc. Am.* **103**, 1048-1068. doi:10.1785/0120120093.

Ktenidou, O-J., F. Cotton, N.A. Abrahamson, and J.G. Anderson (2014). Taxonomy of *κ:* a review of definitions and estimation approaches targeted to applications, *Seism. Res. Lett*., **85** 135-146.

Lanzano, G., C. Felicetta, F. Pacor, D. Spallarossa, and P. Traversa (2022). Generic-to-reference rocks scaling factors for the seismic ground motion in Italy. *Bull. Seism. Soc. Am*., **112** 1583-1606, https://doi.org/10.1785/0120210063.

Lucente, F.P., P. De Gori, L. Margheriti, D. Piccinini, M. Di Bona, C. Chiarraba, and N. Agostinetti (2010). Temporal variation of seismic velocity and anisotropy before the 2009 Mw 6.3 L'Aquila earthquake, Italy. *Geology*, **38** 1015-1018.

Malagnini, L., F.P. Lucente, P. De Gori, A. Akinci, and I. Munafo (2012). Control of pore fluid 654 pressure diffusion on fault failure mode: Insights from the 2009 L'Aquila seismic sequence. *J. Geophys. Res. Solid Earth* **117**. https://doi.org/10.1029/2011JB008911.

Malagnini, L., and T. Parsons (2020). Seismic attenuation monitoring of a critically stressed San Andreas fault, *Geophys. Res. Lett*., https://doi.org/10.1029/2020GL089201.

Malagnini, L., T. Parsons, I. Munafo, S. Mancini, M. Segou, and E.L. Geist (2022). Crustal permeability changes inferred fro seismic attenuation: Impacts on multi-mainshock sequences. *J. Geophys. Res.* (submitted).

Miller, S. A., C. Collettini, L. Chiaraluce, M. Cocco, M. Barchi, B.J. Kaus (2004). Aftershocks driven by a high-pressure CO 2 source at depth. *Nature*, **427**(6976), 724-727.

Nur, A., and J. R. Booker (1972). Aftershocks caused by pore fluid flow? *Science*, **175**(4024): 885–887. https://doi.org/10.1126/science.175. 4024.885

Pacor, F., D. Spallarossa, A. Oth, L. Luzi, R. Puglia, L. Cantore, A. Mercuri, M. D'Amico, and D. Bindi (2016). Spectral models for ground motion prediction in the L'Aquila region (central Italy): evidence for stress-drop dependence on magnitude and depth, *Geophys. J. Int.*, **204** 697-718.

Parolai, S., and D. Bindi (2004). Influence of soil-layer properties on *k* evaluation, *Bull. Seismol. Soc. Am.*, **94**, 349-356.

Perron, V., F., Hollender, P.-Y., Bard, C., Gélis, C., Guyonnet- Benaize, B., Hernandez, O.-J., Ktenidou (2017). Robustness of kappa (κ) measurement in low-to-moderate seismicity areas: insight from a site-specific study in Provence, France. *Bull. Seimol. Soc. Am.* **107**, 2272-2292. doi:10.1785/0120160374

Tung, S., and T. Masterlark (2018). Delay poroelastic triggering of the 2016 October Visso earthquake by the August Amatrice earthquake, Italy. *Geophys. Res. Lett.*, **45**, 221-229.

Van Houtte, C., S., Drouet, F., Cotton (2011). Analysis of the origins of K (Kappa) to compute hard rock to rock adjustment factors for GMPEs. *Bull. Seimol. Soc. Am*. **101**, 2926-2941. doi:10.1785/0120100345.

Wells, D.L., and K.J. Coppersmith (1994). New empirical relationships among magnitude, rupture length, rupture width, rupture area, and surface displacement. *Bull. Seism. Soc. Am*., **84**, 974-1002.

Raúl R. Castro[1]

[1]*Centro de Investigación Científica y de Educación Superior de Ensenada (CICESE), División Ciencias de la Tierra, Departamento de Sismología, Carretera Tijuana-Ensenada No. 3918, 22860 Ensenada, Baja California, México.* raul@cicese.mx

Daniele Spallarossa[2]

[2] *Universita degli Studi di Genova, DISTAV, Genova, Italy.* daniele@dipteris.unige.it

Francesca Pacor[3]

[3]*Istituto Nazionale di Geofísica e Vulcanologia,Via Alfonso Corti 12, Milan 20133, Italy.* Francesca.pacor@ingv.it

Leonardo Colavitti[3]

[3]*Istituto Nazionale di Geofísica e Vulcanologia,Via Alfonso Corti 12, Milan 20133, Italy.* Leonardo.colavitti@ingv.it

Giovanni Lanzano[3]

[3]*Istituto Nazionale di Geofísica e Vulcanologia,Via Alfonso Corti 12, Milan 20133, Italy.* Giovanni.lanzano@ingv.it

Claudia A. Vidales-Basurto[4]

[4]*Centro de Investigación en Matemáticas, A.C. (CIMAT). Calzada de la Plenitud 103, Aguascalientes, 20200 México.* Rammstein_immer16@hotmail.com

Sara Sgobba[3]

[3]*Istituto Nazionale di Geofísica e Vulcanologia,Via Alfonso Corti 12, Milan 20133, Italy.*

Sara.sgobba@ingv.it

## List of Figure Captions

**Figure 1**. **(a)** Maps of the distribution of earthquakes analyzed with magnitudes ranging between 3.4 and 6.5. The red stars correspond to the epicenters of the Mw=6.0 Amatrice ($42^0$ 42'N, $13^0$ 13.8'E), the Mw=5.9 Visso ($42^0$ 54.6'N, $13^0$ 7.8'E) and the Mw=6.5 Norcia ($42^0$ 49.8'N, $13^0$ 6.6'E) earthquakes. **(b)** Map with recording stations.

**Figure 2.** Magnitude-distance distribution of the recordings of the dataset used.

**Figure 3**. On the left is the average source-station *S*-wave path kappa $\tilde{\kappa}(r)$ calculated from the records of the Amatrice earthquake (Mw 6.0) of August 24, 2016 (solid line), from foreshock (asterisk), from 15 days of aftershocks (circles), from 30 days of aftershocks (triangles), from three months of aftershocks (crosses) and from two months of aftershocks (diamonds). The $\tilde{\kappa}(r)$ calculated using foreshocks of the Norcia earthquake is represented with filled squares. On the right is $\tilde{\kappa}(r)$ calculated from foreshocks (continuous line) and aftershocks (circles) of the Visso earthquake (Mw 5.9) of October 26, 2016.

**Figure 4.** Kappa near the source ($\kappa_s$) computed from aftershocks that occurred during 15 days after the Amatrice earthquake (Mw 6.0) of August 24, 2016.

**Figure 5.** Spatial distribution of near-source attenuation ($\kappa_s$) of the aftershocks occurred during the 15 days after the Amatrice earthquake (Mw 6.0) of August 24, 2016 (blue star).

**Figure 6**. Focal depth (left) and magnitude (right) versus kappa near the source ($\kappa_s$) from the aftershocks occurred during the 15 days after the Amatrice earthquake (Mw 6.0) of August 24, 2016. The continuous line on the left is the linear regression least-square fit using all data points.

**Figure 7**. Average source-station *S*-wave path kappa $\tilde{\kappa}(r)$ calculated from the records of the Norcia earthquake (Mw 6.5) of October 30, 2016 (triangles), from foreshocks (black continuous line), and from aftershocks (stars).

**(a)**

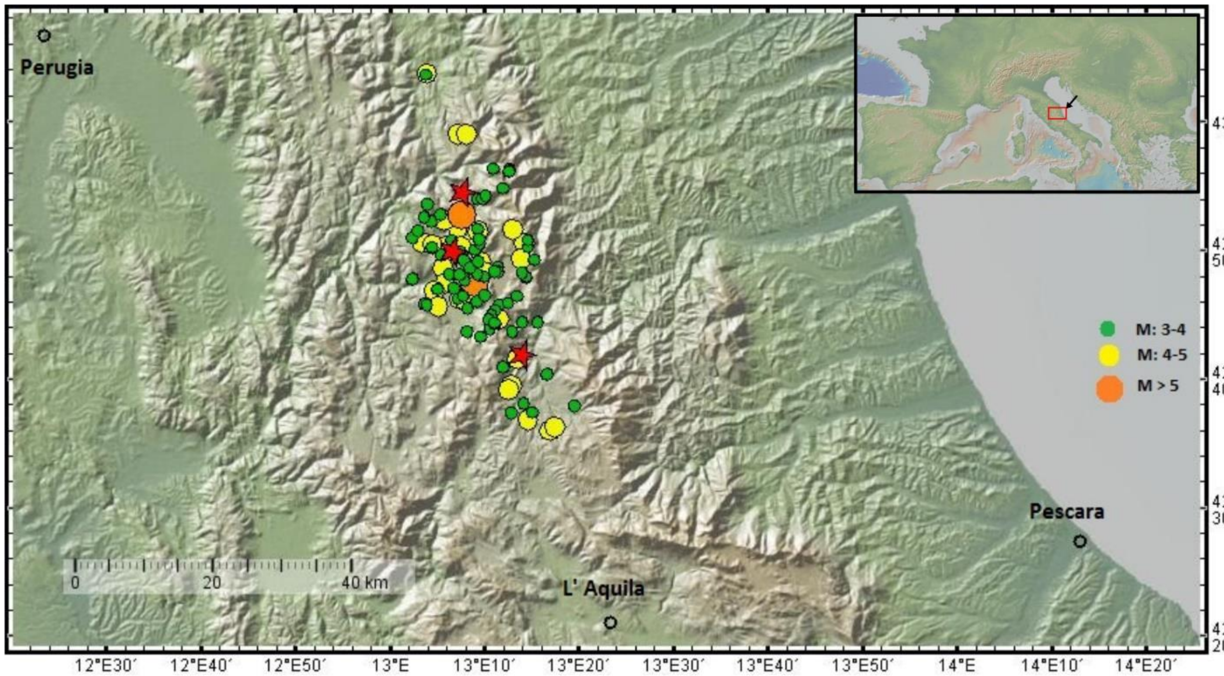

Perugia
43°N
42°N 50′
M: 3-4
M: 4-5
M > 5
42°N 40′
42°N 30′
Pescara
0 20 40 km
L' Aquila
42°N 20′
12°E30′ 12°E40′ 12°E50′ 13°E 13°E10′ 13°E20′ 13°E30′ 13°E40′ 13°E50′ 14°E 14°E10′ 14°E20′


**(b)**

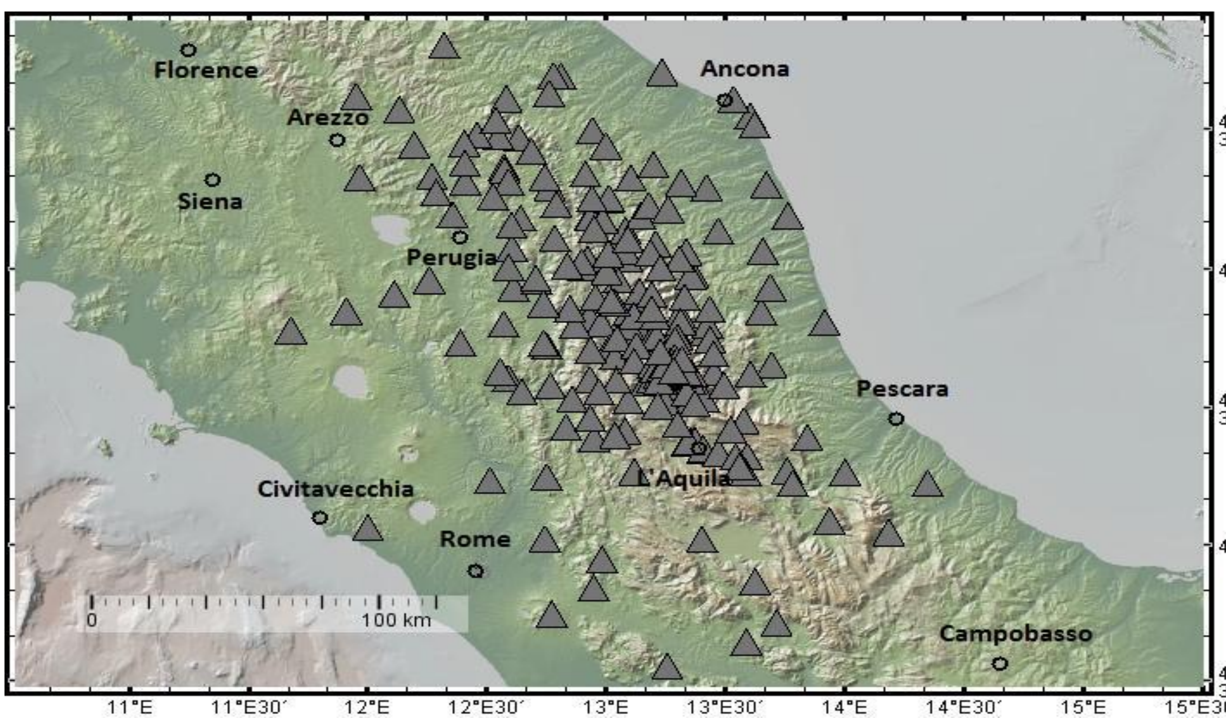

Florence
Ancona
Arezzo
Siena
Perugia
43°N 30′
43°N
Pescara
42°N 30′
L'Aquila
Civitavecchia
Rome
42°N
0 100 km
Campobasso
41°N 30′
11°E 11°E30′ 12°E 12°E30′ 13°E 13°E30′ 14°E 14°E30′ 15°E 15°E30′

**Figure 1**. **(a)** Maps of the distribution of earthquakes analyzed with magnitudes ranging between 3.4 and 6.5. The red stars correspond to the epicenters of the Mw=6.0 Amatrice ($42^0$ 42'N, $13^0$ 13.8'E), the Mw=5.9 Visso ($42^0$ 54.6'N, $13^0$ 7.8'E) and the Mw=6.5 Norcia ($42^0$ 49.8'N, $13^0$ 6.6'E) earthquakes. **(b)** Map with recording stations.

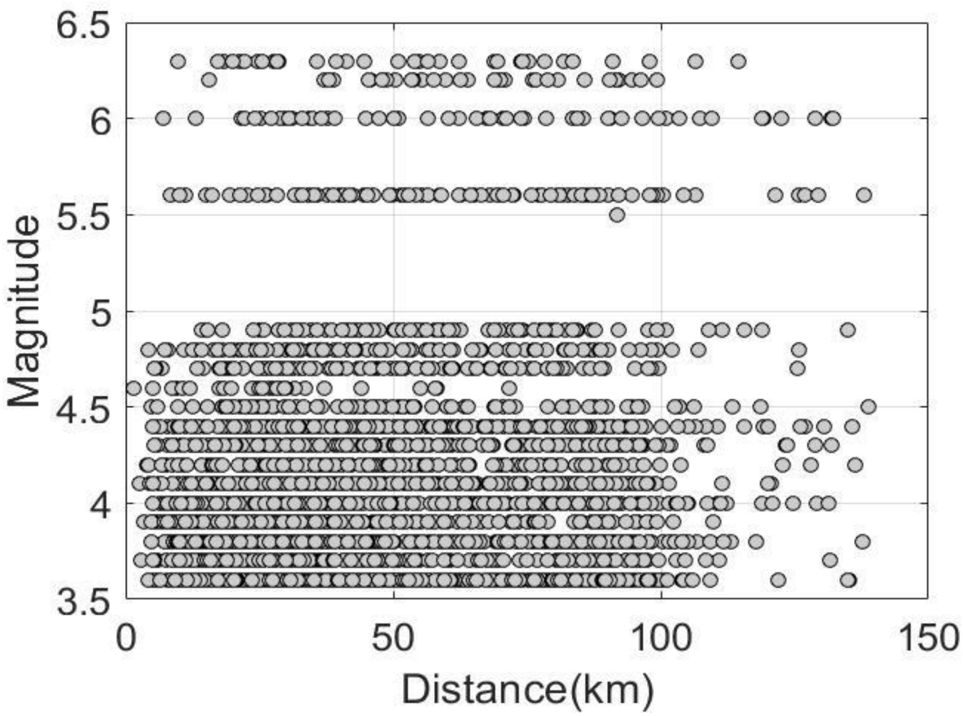


**Figure 2.** Magnitude-distance distribution of the recordings of the dataset used.

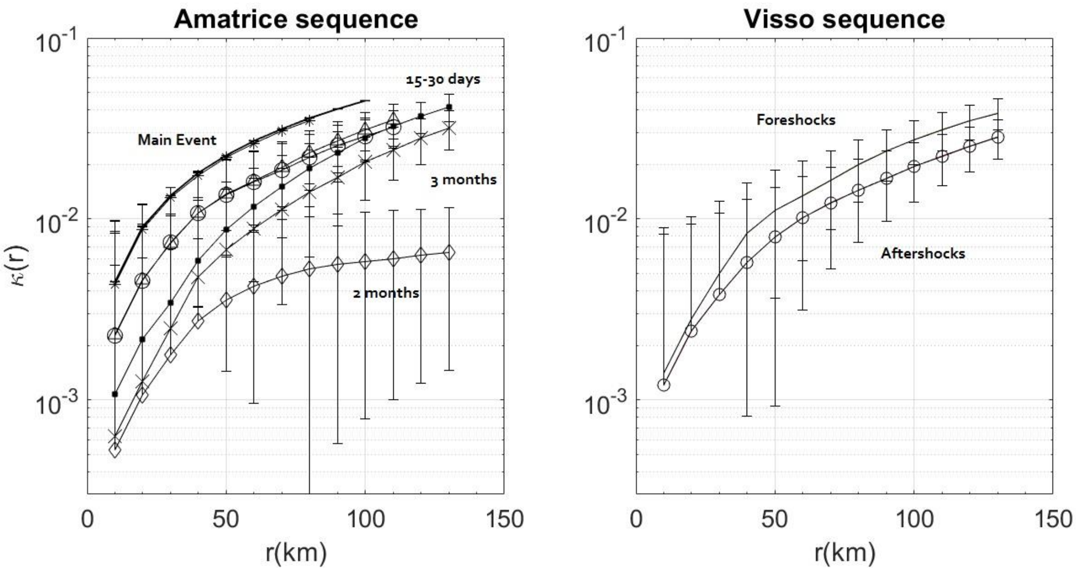


**Figure 3**. On the left is the average source-station *S*-wave path kappa $\tilde{\kappa}(r)$ calculated from the records of the Amatrice earthquake (Mw 6.0) of August 24, 2016 (solid line), from foreshock (asterisk), from 15 days of aftershocks (circles), from 30 days of aftershocks (triangles), from three months of aftershocks (crosses) and from two months of aftershocks (diamonds). The $\tilde{\kappa}(r)$ calculated using foreshocks of the Norcia earthquake is represented with filled squares. On the right is $\tilde{\kappa}(r)$ calculated from foreshocks (continuous line) and aftershocks (circles) of the Visso earthquake (Mw 5.9) of October 26, 2016.

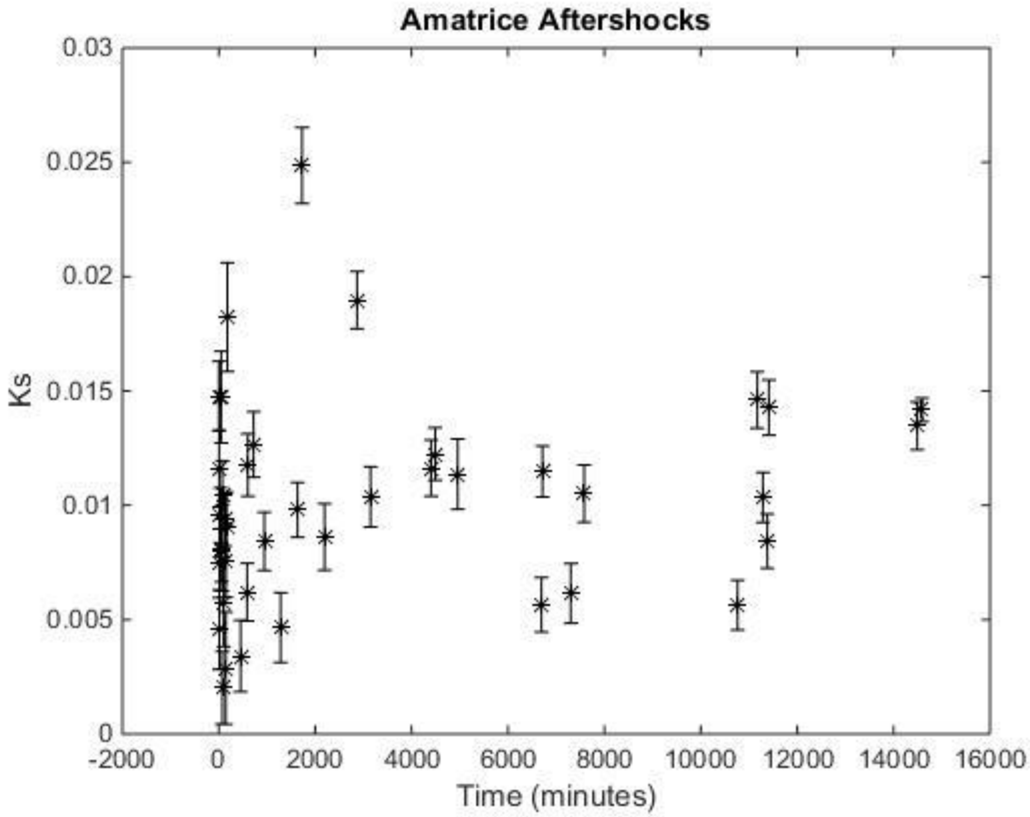


**Figure 4.** Kappa near the source ($\kappa_s$) computed from aftershocks that occurred during 15 days after the Amatrice earthquake (Mw 6.0) of August 24, 2016.

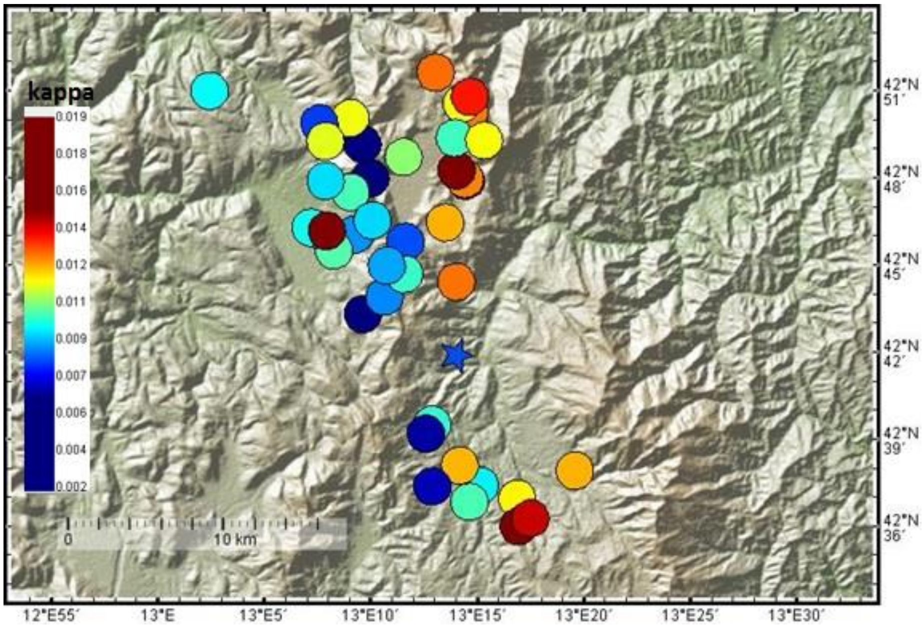


**Figure 5.** Spatial distribution of near-source attenuation ($\kappa_s$) of the aftershocks occurred during the 15 days after the Amatrice earthquake (Mw 6.0) of August 24, 2016 (blue star).

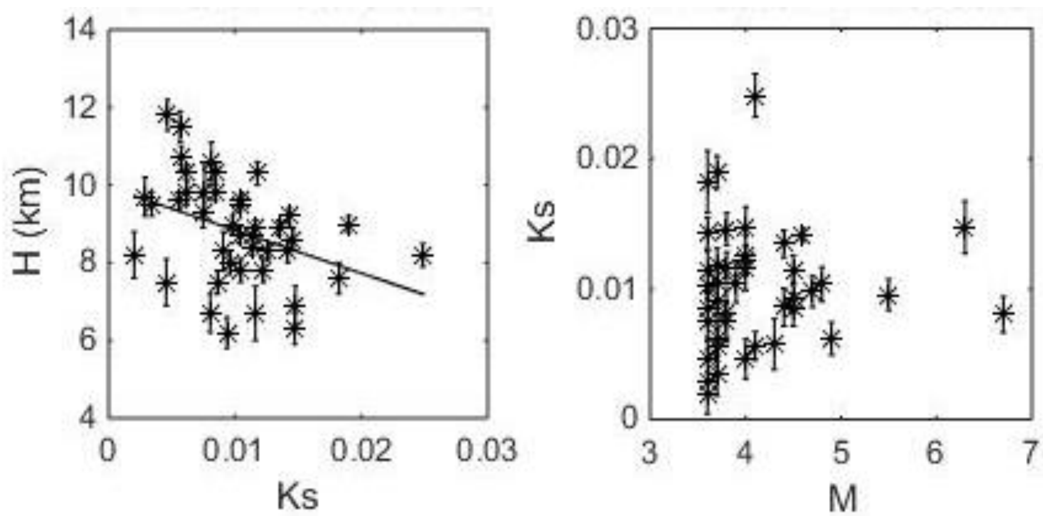


**Figure 6**. Focal depth (left) and magnitude (right) versus kappa near the source ($\kappa_s$) from the aftershocks occurred during the 15 days after the Amatrice earthquake (Mw 6.0) of August 24, 2016. The continuous line on the left is the linear regression least-square fit using all data points.

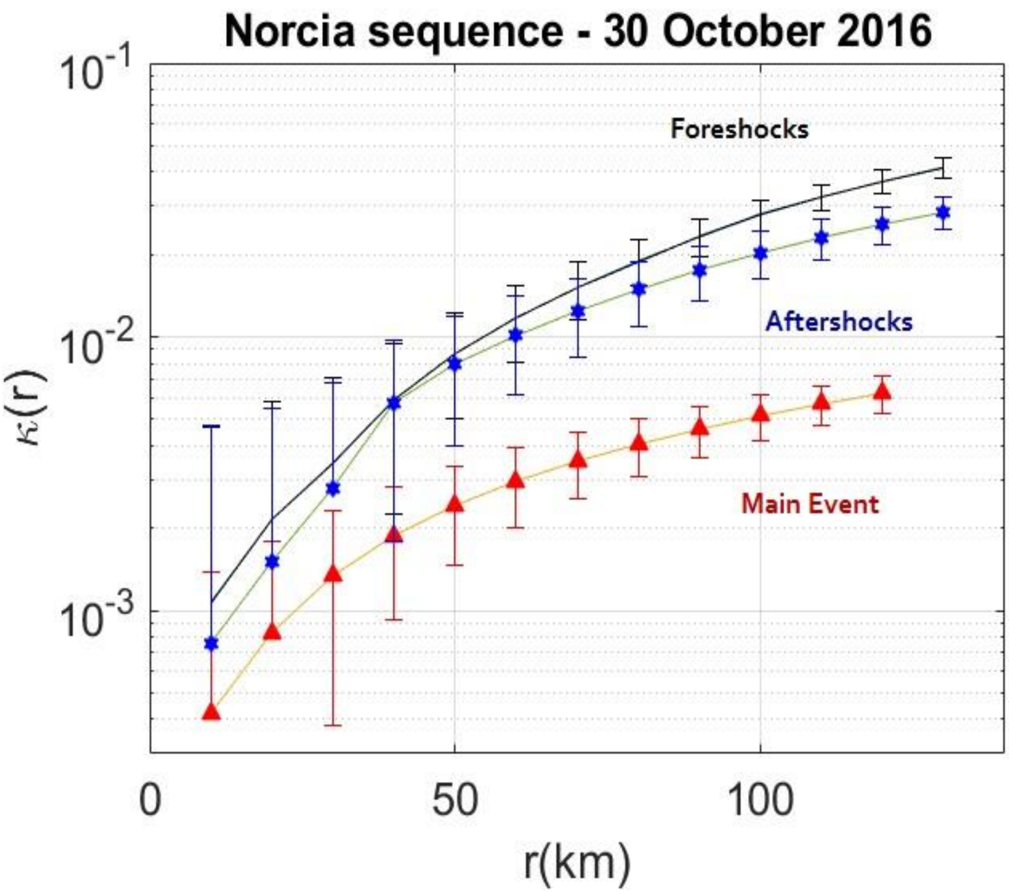


**Figure 7**. Average source-station *S*-wave path kappa $\tilde{\kappa}(r)$ calculated from the records of the Norcia earthquake (Mw 6.5) of October 30, 2016 (triangles), from foreshocks (black continuous line), and from aftershocks (stars).

Figure 1a

Click here to access/download;Figure;Fig1a_BSSA107.png

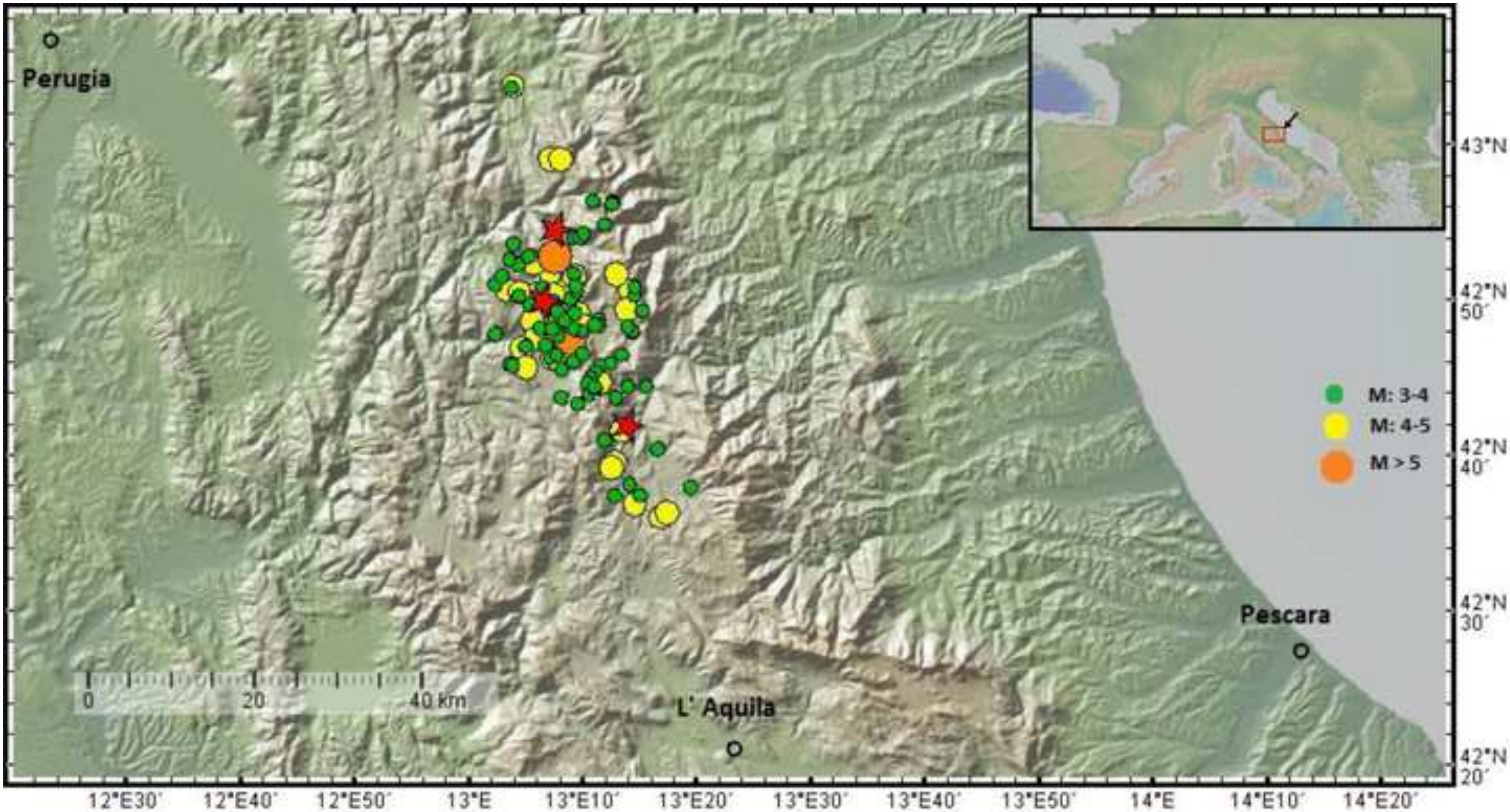

Figure 1b

Click here to access/download;Figure;Fig1b_BSSA107.jpg

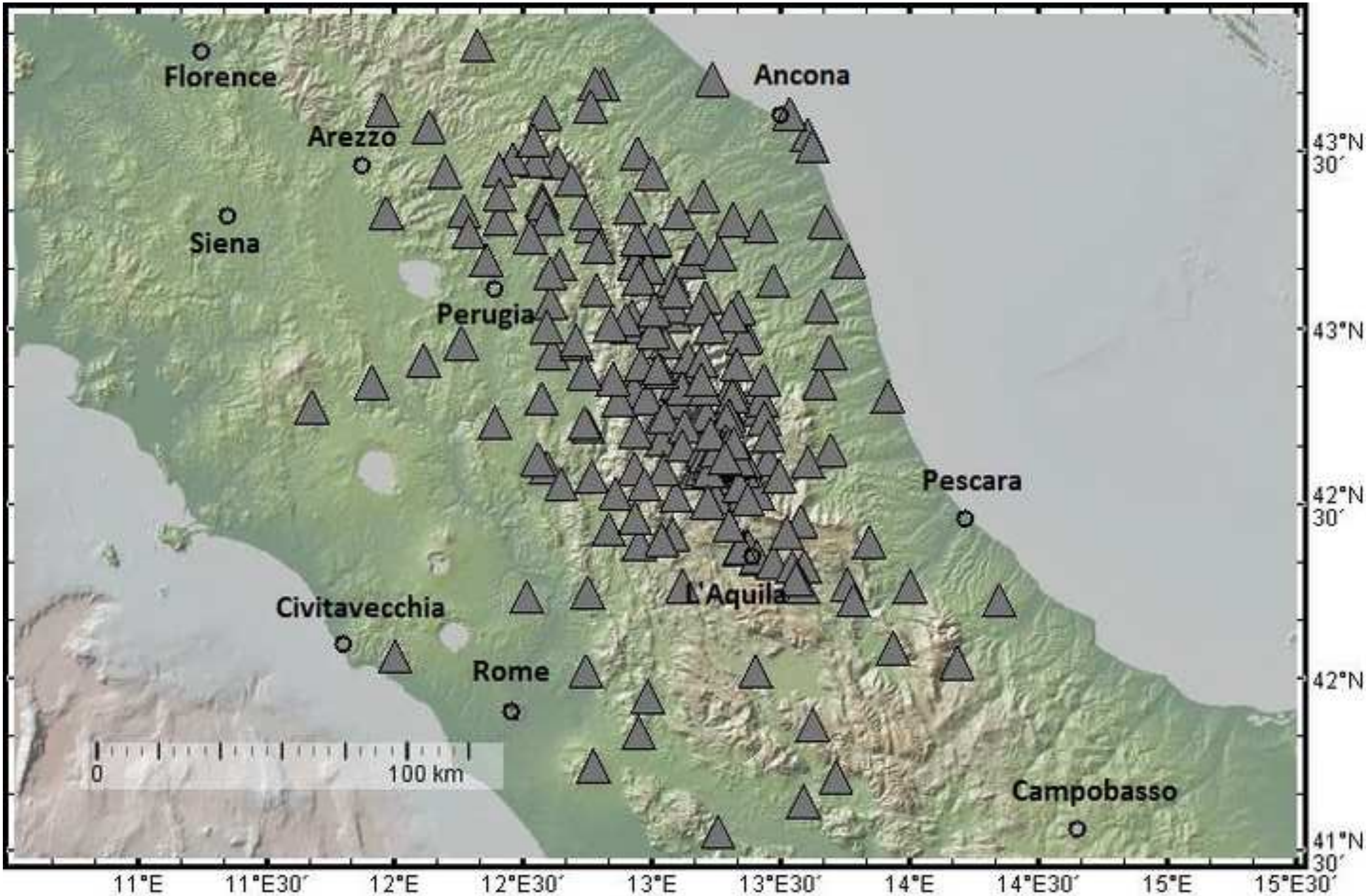

Figure 2



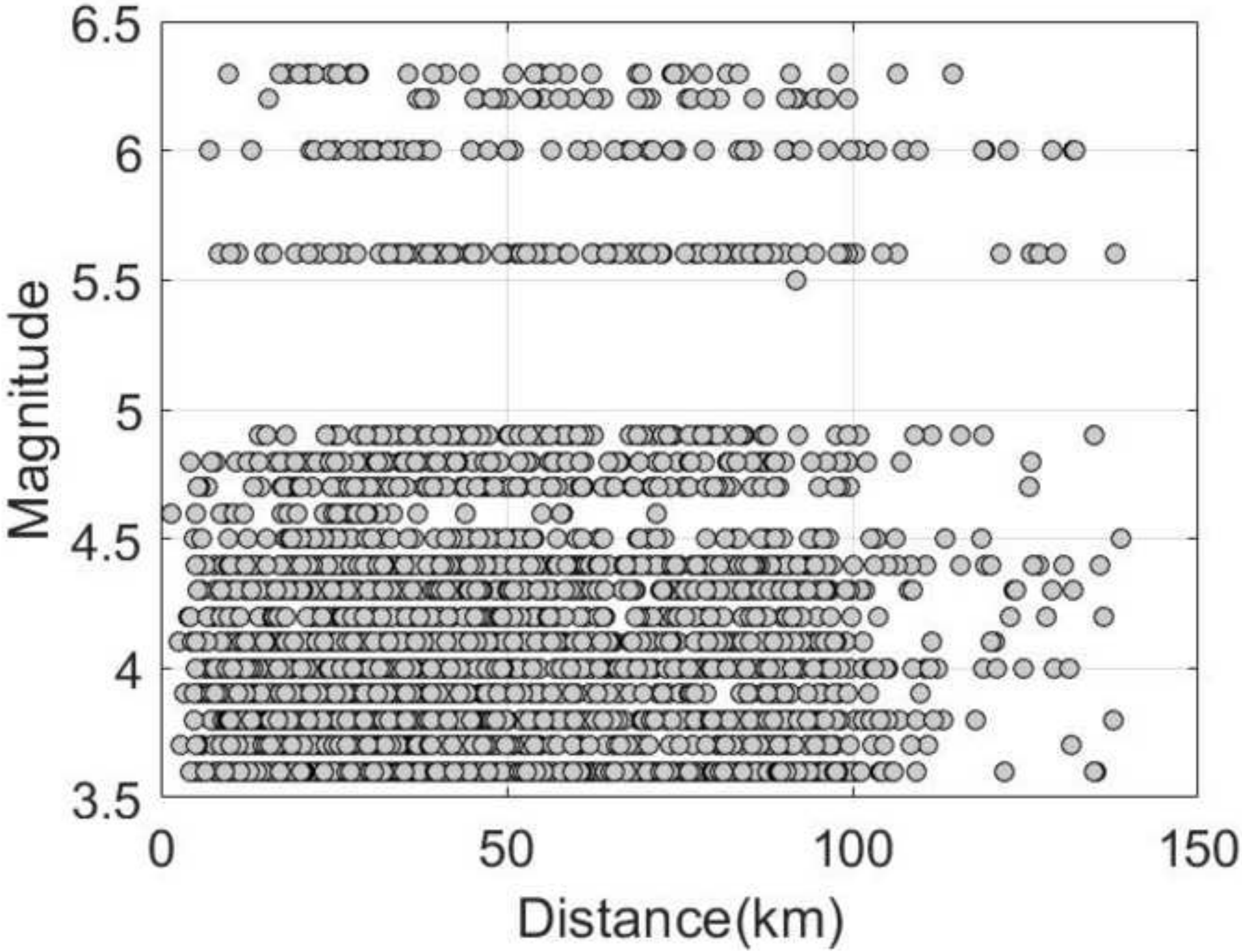

Figure 3



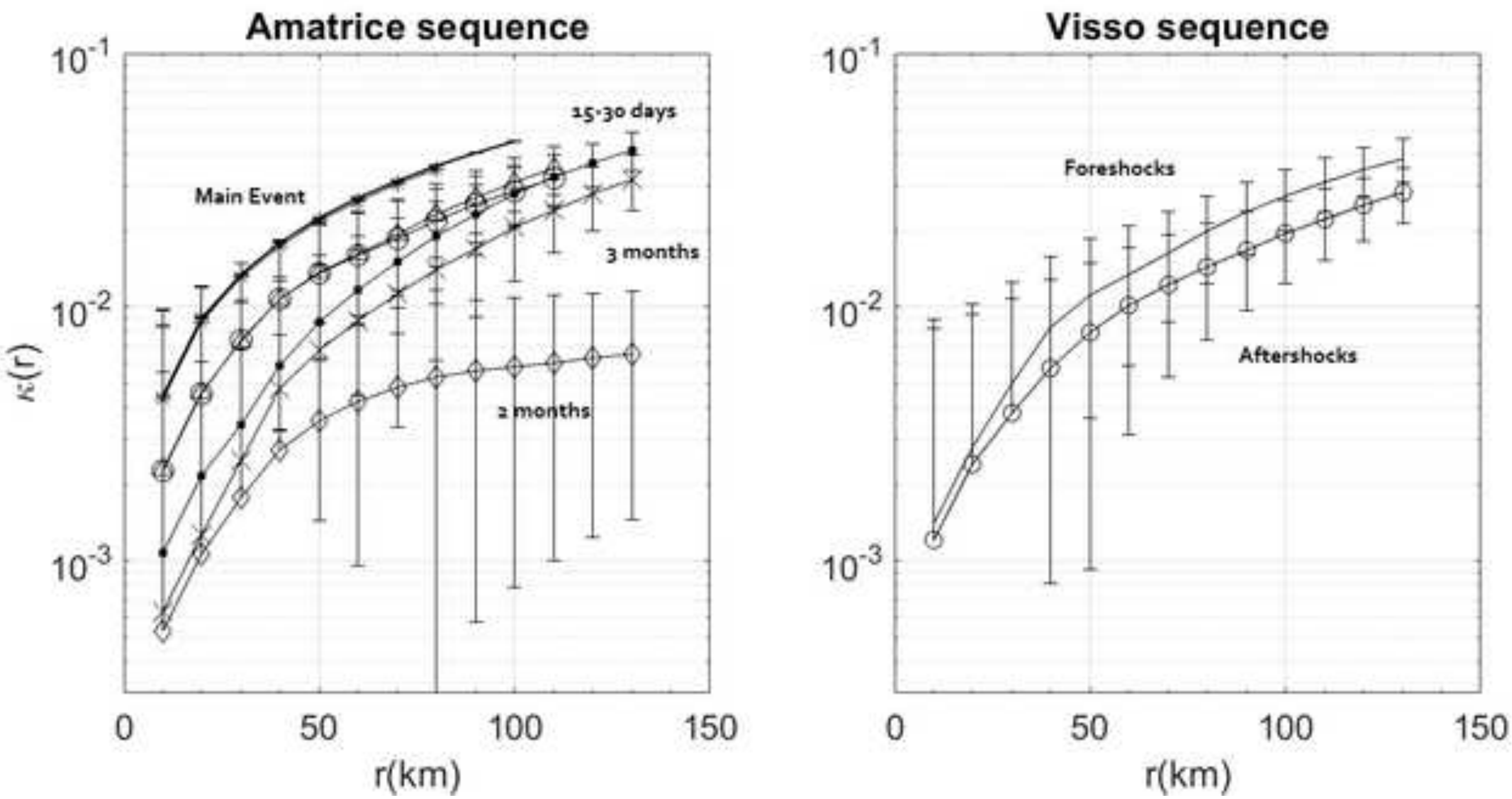
Amatrice sequence
Visso sequence
15-30 days
Main Event
3 months
2 months
Foreshocks
Aftershocks
κ(r)
r(km)
r(km)

Figure 4



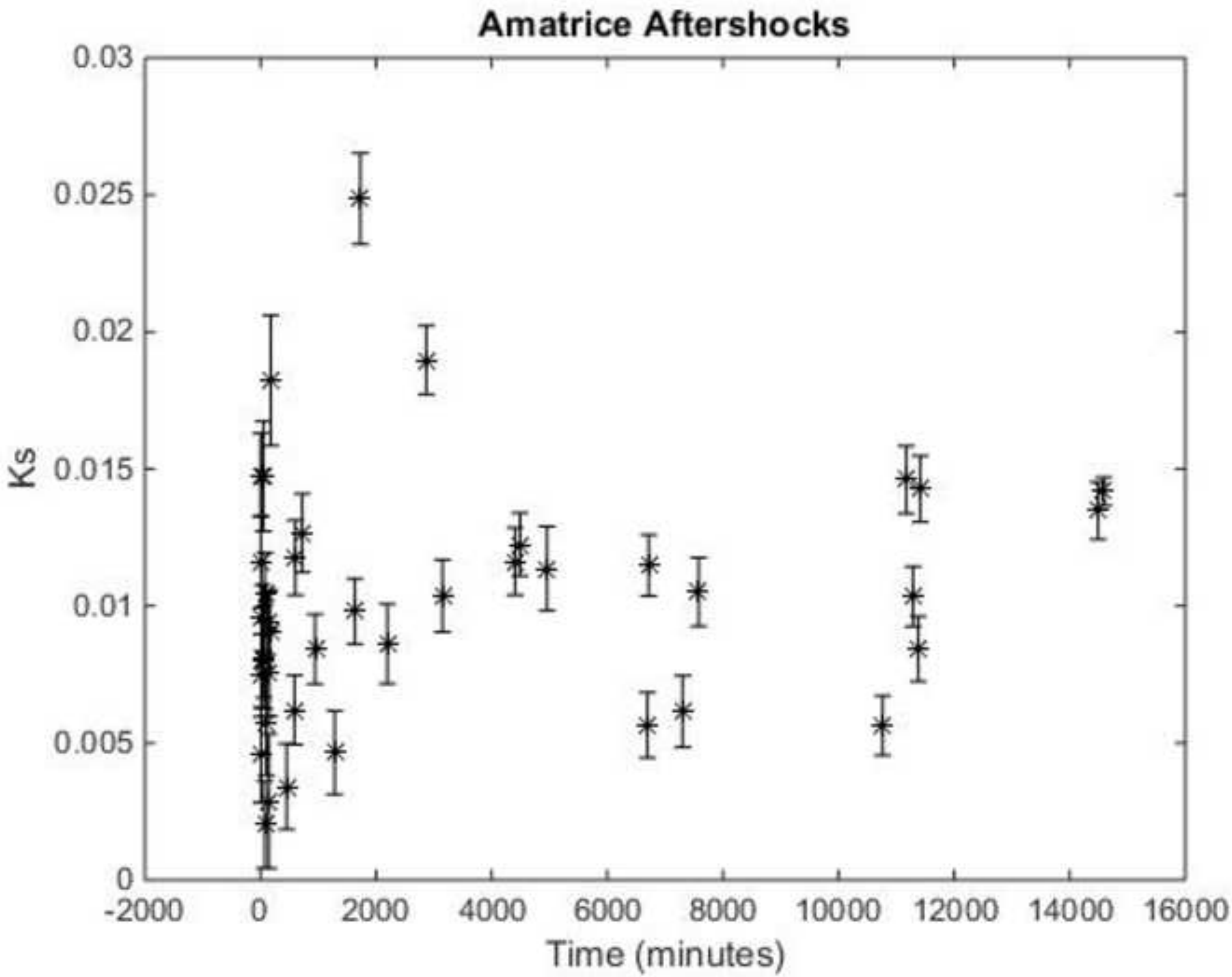
Amatrice Aftershocks
0.03
0.025
0.02
0.015
0.01
0.005
0
Ks
-2000
0
2000
4000
6000
8000
10000
12000
14000
16000
Time (minutes)

Figure 5 Click here to access/download;Figure;Fig5_BSSA107.jpg

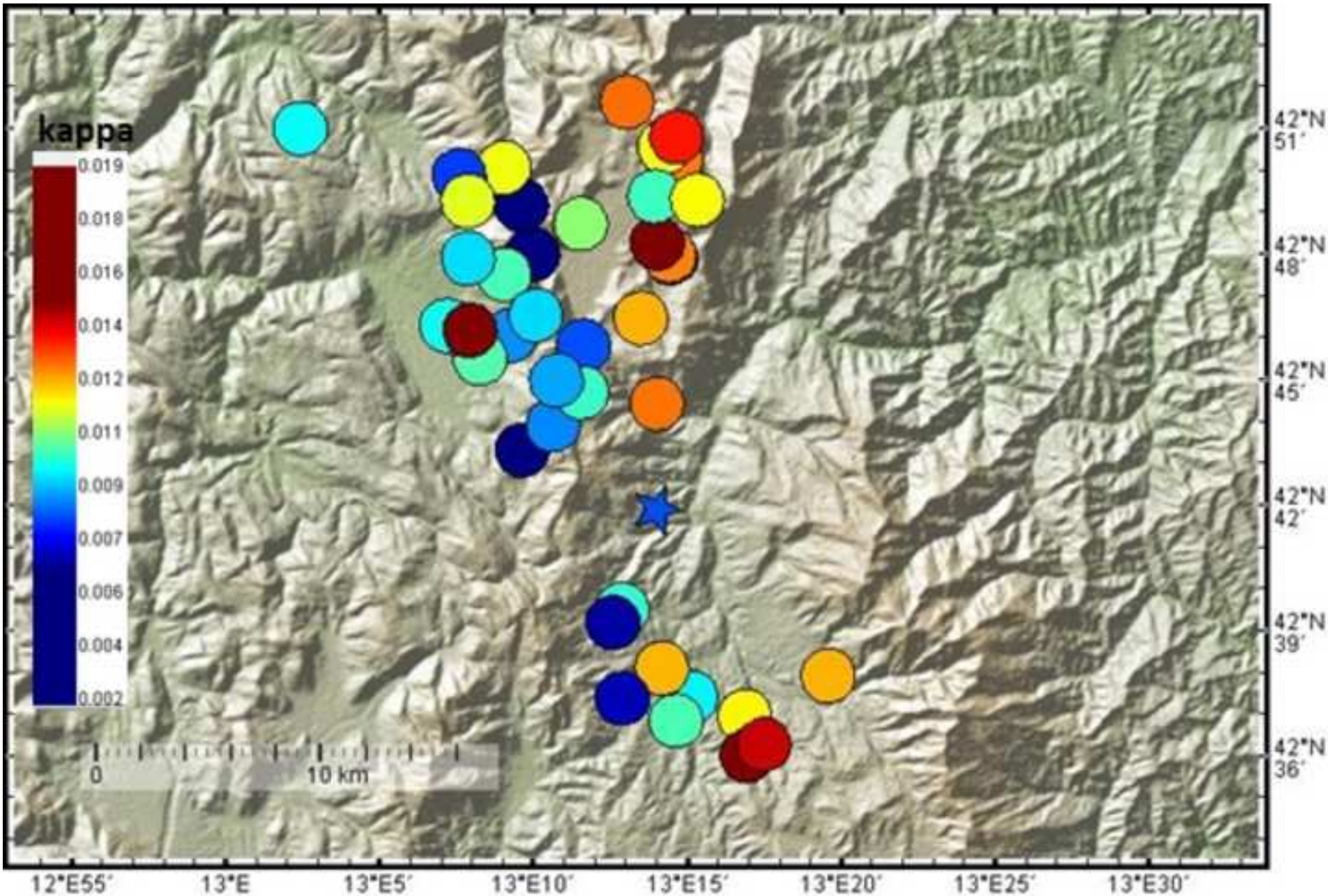

Figure 6



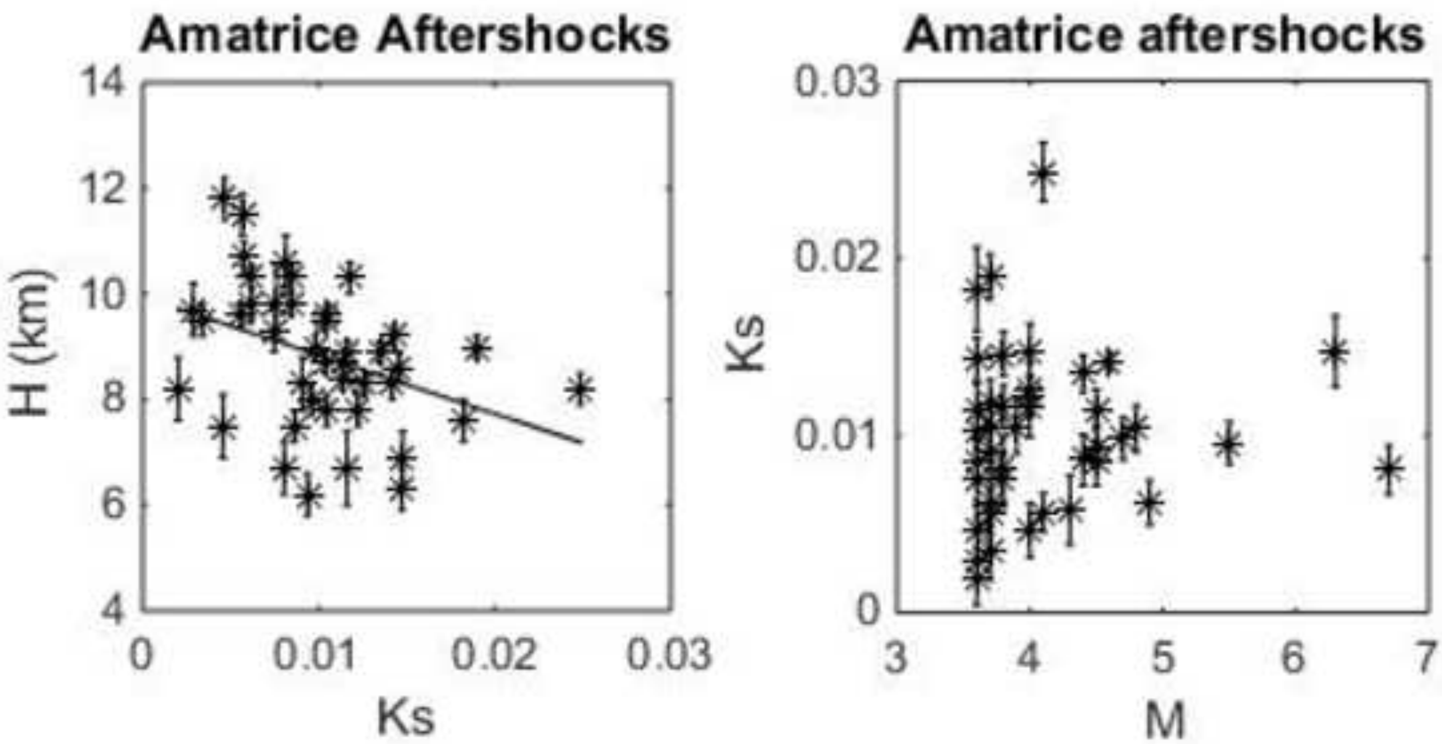

Amatrice Aftershocks
H (km)
14
12
10
8
6
4
0
0.01
0.02
0.03
Ks
Amatrice aftershocks
Ks
0.03
0.02
0.01
0
3
4
5
6
7
M

 

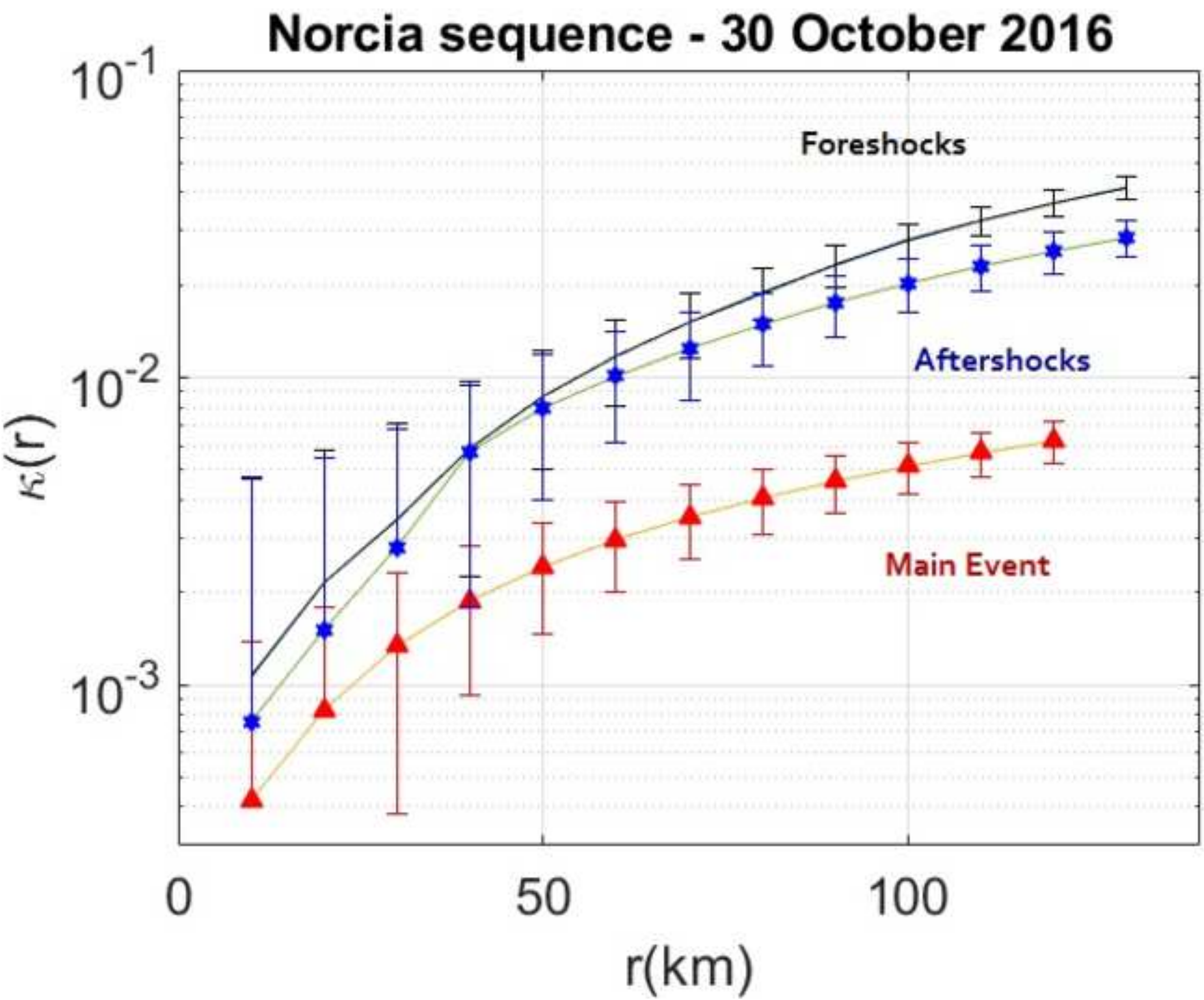
Norcia sequence - 30 October 2016
$10^{-1}$
$10^{-2}$
$10^{-3}$
κ(r)
Foreshocks
Aftershocks
Main Event
0
50
100
r(km)